

Magnetic Field Alignable Domains in Phospholipid Vesicle Membranes Containing Lanthanides

Paul Beck,[†] Marianne Liebi,^{*,†} Joachim Kohlbrecher,[‡] Takashi Ishikawa,[§] Heinz Rüegger,^{#,||} Helmut Zepik,[⊥] Peter Fischer,[†] Peter Walde,[⊥] and Erich Windhab[†]

Laboratory of Food Process Engineering, ETH Zurich, Schmelzbergstrasse 9, 8092 Zurich, Switzerland, Laboratory for Neutron Scattering, ETH Zurich & Paul Scherrer Institute, 5232 Villigen PSI, Switzerland, Department of Biology, ETH Zurich, Schafmattstrasse 20, 8093 Zurich, Switzerland, Laboratory for Inorganic Chemistry, ETH Zurich, Wolfgang-Pauli-Strasse 10, 8093 Zurich, Switzerland, and Department of Materials, ETH Zurich, Wolfgang-Pauli-Strasse 10, 8093 Zurich, Switzerland

Received: August 3, 2009; Revised Manuscript Received: November 25, 2009

Magnetic fields were applied as a structuring force on phospholipid-based vesicular systems, using paramagnetic lanthanide ions as magnetic handles anchored to the vesicle membrane. Different vesicle formulations were investigated using small angle neutron scattering (SANS) in a magnetic field of up to 8 T, cryo-transmission electron microscopy (cryo-TEM), ³¹P NMR spectroscopy, dynamic light scattering (DLS), and permeability measurements with a fluorescent water-soluble marker (calcein). The investigated vesicle formulations consisted usually of 80 mol % of the phospholipid 1-palmitoyl-2-oleoyl-sn-glycero-3-phosphocholine (POPC) and 20 mol % of a chelator lipid (DMPE-DTPA; 1,2-dimyristoyl-sn-glycero-3-phosphoethanolamine-diethylenetriaminepentaacetate) with complexed lanthanide ions (Tm^{3+} , Dy^{3+} , or La^{3+}), and the total lipid concentration was 15 mM. Vesicles containing the paramagnetic lanthanide Tm^{3+} or Dy^{3+} exhibited a temperature-dependent response to magnetic fields, which can be explained by considering the formation of lipid domains, which upon reaching a critical size become alignable in a magnetic field. The features of this “magnetic field alignable domain model” are as follows: with decreasing temperature (from 30 to 2.5 °C) solid domains, consisting mainly of the higher melting phospholipid (DMPE-DTPA•lanthanide), begin to form and grow in size. The domains assemble the large magnetic moments conferred by the lanthanides and orient in magnetic fields. The direction of alignment depends on the type of lanthanide used. The domains orient with their normal parallel to the magnetic field with thulium (Tm^{3+}) and perpendicular with dysprosium (Dy^{3+}). No magnetic field alignable domains were observed if DMPE-DTPA is replaced either by POPE-DTPA (1-palmitoyl-2-oleoyl-sn-glycero-3-phosphoethanolamine-diethylenetriamine-pentaacetate) or by DMPC (1,2-dimyristoyl-sn-glycero-3-phosphocholine).

Introduction

Magnetic field effects on biological molecules are rarely observed, due to the small diamagnetic susceptibility of individual molecules. In lipid self-assembly systems, such as phospholipid bilayers, in which the molecules are aggregated parallel to each other, the anisotropy of the diamagnetic susceptibility is additive,^{1,2} and a magnetic orientation perpendicular to the magnetic field becomes possible. A well-known system where this magnetic orientation has been exploited is a bicellar mixture of long- and short-chain phospholipids used in NMR studies of transmembrane proteins.^{3–7} By doping these planar aggregates with paramagnetic lanthanide ions with a large magnetic moment, the responsiveness to magnetic fields can be enhanced significantly.^{8–11} The orientability of paramagnetic macromolecules or macromolecules which contain paramagnetic tags (such as lanthanides) is routinely used in NMR spectroscopy. Protein structure determinations and in particular protein/ligand interaction studies can be carried out by measuring

orientation-dependent parameters as residual dipolar couplings (RDC) in field-aligned systems.^{12–14}

The paramagnetic lanthanide ions can be classified, depending on the sign of the magnetic anisotropy $\Delta\chi$. Phospholipids doped with Ce^{3+} , Pr^{3+} , Nd^{3+} , Sm^{3+} , Tb^{3+} , Dy^{3+} , or Ho^{3+} have a large negative $\Delta\chi$ resulting in a preferred orientation with the long molecular axis perpendicular to the magnetic field. On the other hand, $\Delta\chi$ of phospholipids doped with Eu^{3+} , Er^{3+} , Tm^{3+} , or Yb^{3+} becomes positive, resulting in a preferred alignment in the direction of the magnetic field.⁷ The trivalent cation of lanthanum (La^{3+}) is diamagnetic and does not alter the magnetic anisotropy of the phospholipids. As shown by Prosser et al. (1998),^{10,11} the lanthanide cations can be anchored to the membrane with the use of a chelator covalently bound to a phospholipid, e.g., DMPE-DTPA (1,2-dimyristoyl-sn-glycero-3-phosphoethanolamine-diethylenetriaminepentaacetate). Complexed with gadolinium (Gd^{3+}), such vesicles have been investigated as a potential MRI contrast marker.¹⁵

In this study, we investigated the effect of magnetic fields on phospholipid vesicles containing a chelator-lipid with complexed paramagnetic lanthanides with large magnetic anisotropy. Possible magnetic field effects considered were vesicle deformation, aggregation/fusion, budding/fission, permeability alteration, and lateral lipid segregation. For pure phospholipid vesicles, in

* Corresponding author. E-mail: marianne.liebi@ilw.agrl.ethz.ch.

[†] Laboratory of Food Process Engineering.

[‡] Laboratory for Neutron Scattering.

[§] Department of Biology.

[#] Laboratory for Inorganic Chemistry.

[⊥] Department of Materials.

^{||} Heinz Rüegger passed away on June 28, 2009.

the absence of any added lanthanides, a few such effects have been described. It has been shown for example that vesicles can slightly be deformed and oriented in magnetic fields.^{16–20} The influence of magnetic fields on permeability has been claimed by Tenforde and Liburdy,^{21,22} Kurashima et al.²³ reported on magnetic field induced fusion of vesicles.

Lateral lipid segregation and domain formation in the absence of magnetic fields have been described for multicomponent phospholipid vesicles from mixtures of DOPC (1,2-dioleoyl-*sn*-glycero-3-phosphocholine), DPPC (1,2-dipalmitoyl-*sn*-glycero-3-phosphocholine), and cholesterol. These systems have gained increasing interest in recent years as models for lipid rafts in biomembranes.^{24–36}

Here we report on investigations of different formulations of vesicles analyzed at different temperatures and under different magnetic field strengths. As the standard sample we used vesicles composed of 80% POPC (1-palmitoyl-2-oleoyl-*sn*-glycero-3-phosphocholine) and 20% DMPE-DTPA with complexed thulium ions (Tm^{3+}). Additional formulations varied in one of the three components or in the ratio of POPC to DMPE-DTPA. We used small angle neutron scattering (SANS) under magnetic field, complemented by direct observation of the structures at two different temperatures by cryo-transmission electron microscopy (cryo-TEM). Additional information was gained through permeability measurements with calcein, ³¹P NMR, and dynamic light scattering (DLS).

Materials and Methods

Materials. The phospholipids, 1,2-dimyristoyl-*sn*-glycero-3-phosphocholine (DMPC), 1-palmitoyl-2-oleoyl-*sn*-glycero-3-phosphocholine (POPC), and 1,2-dimyristoyl-*sn*-glycero-3-phosphoethanolamine-diethylenetriaminepentaacetate (DMPE-DTPA), were purchased as chloroform solutions from Avanti Polar Lipids (Alabaster, AL) and used without further purification. 1-Palmitoyl-2-oleoyl-*sn*-glycero-3-phosphoethanolamine-diethylenetriaminepentaacetate (POPE-DTPA) was synthesized according to a modified approach described by Torchilin et al.³⁷ $TmCl_3$ (99.9%), $LaCl_3$ (99.9%), $DyCl_3$ (99.9%), calcein disodium salt (99.9%), Sepharose 4B, and D_2O (99.9 atom % D) used for ³¹P NMR samples and D_2O (99.9 atom % D, containing 0.05 wt % 3-(trimethylsilyl)propionic-2.2.3.3-*d*₄ acid, sodium salt) used for SANS and cryo-TEM samples were from Sigma-Aldrich (Buchs, Switzerland). Stock solutions of 10 mM $TmCl_3$ and $DyCl_3$ in MeOH and of 10 mM $LaCl_3$ in MeOH/ H_2O (19/1 v/v) were prepared.

Vesicle Preparation. After weighing the appropriate amounts of the lipid and lanthanide stock solutions into a round-bottom flask, chloroform and methanol were evaporated under a rotary evaporator followed by residual solvent removal under high vacuum overnight. The formed dry lipid film was hydrated with D_2O and vortexed until a homogeneous suspension was obtained. Five repeated freeze-thaw cycles were carried out by plunging the flask into liquid nitrogen followed by slow heating above the phase transition temperature (about 40–45 °C). To obtain a homogeneous vesicle size distribution and to reduce multilamellarity, an extrusion step through polycarbonate membranes was carried out.³⁸ The extrusion was performed under nitrogen at room temperature with “The Extruder” from Lipex Biomembranes (Vancouver, Canada) and Nucleopore polycarbonate membranes from Sterico (Dietikon, Switzerland).^{38,39} The suspension was first passed 10 times through a membrane with 200 nm pores, followed by 10 times through a membrane with 100 nm pores. All samples were prepared with a total lipid concentration of 15 mM. The standard sample consisted of a

POPC:DMPE-DTPA:lanthanide mixture with a molar ratio of 4:1:1. The vesicle samples are denoted as POPC/DMPE-DTPA·Tm, POPC/DMPE-DTPA·La, or POPC/DMPE-DTPA·Dy in the text, depending on the lanthanide used, and POPC/DMPE-DTPA if no lanthanide was complexed. The sample denoted as POPC/POPE-DTPA·Tm was prepared with POPE-DTPA instead of DMPE-DTPA, in the same molar ratio. One sample with a DMPC:DMPE-DTPA:Tm ratio of 3:2:2 was prepared, denoted as DMPC/highDMPE-DTPA·Tm. Furthermore, one pure phosphatidylcholine sample, POPC/DMPC, with a lipid molar ratio of 4:1 was prepared. All samples were stored at room temperature before measurements and were stable over a period of at least two weeks. Vesicle diameter was determined by using dynamic light scattering (see Supporting Information).

SANS. SANS experiments were performed on the SANS-I beamline at PSI, Villigen, Switzerland, using a superconductive magnet with a horizontal field of 8 T perpendicular to the neutron beam, as described previously.⁴⁰ Data were collected on a two-dimensional detector covering a momentum transfer q of $0.003 \leq q \leq 0.15 \text{ \AA}^{-1}$. After correction for background, empty cell scattering, and detector efficiency, the 2D intensity maps were radial averaged and sectoral averaged with an opening angle of 15° perpendicular and parallel to the magnetic field direction.

Cryo-TEM. The samples were analyzed by cryo-transmission electron microscopy (cryo-TEM) following the procedure described previously.⁴⁰ The samples were held at two different temperatures (22 and 5 °C) prior to quick-freezing in liquid ethane at the temperature of liquid nitrogen. For samples frozen from room temperature, a VitrobotTM apparatus (FEI company, Eindhoven, The Netherlands) was used. For samples frozen from 5 °C, the manual blotting apparatus was transferred into a cold room with $5 \text{ }^\circ\text{C} \pm 0.5 \text{ }^\circ\text{C}$, and the sample was precooled in a water bath. Every part of the equipment coming into contact with the sample was held for at least 4 h in the cold room prior to sample freezing. The grids were examined using a cryo-holder (model 626, Gatan, USA) and a Tecnai G2 F20 microscope (FEI company) equipped with a field emission gun and Tridem energy filter (Gatan) operated at an accelerating voltage of 200 kV. The data were recorded by a 2048 × 2048 CCD camera (Gatan).

NMR. ³¹P NMR spectra were acquired at 283 MHz using a Bruker Biospin spectrometer operating with a 16.4 T field. Temperature was adjusted with a flow of cold nitrogen gas, heated to the appropriate temperature.

Permeability Measurements. For permeability measurements, vesicles were prepared with the same method as described above, but instead of rehydrating the films with D_2O , an aqueous 50 mM calcein solution of pH 7 was used. At this concentration, the fluorescence of calcein is low due to self-quenching.⁴¹ After extrusion, size exclusion chromatography through a Sepharose 4B column was performed to remove unencapsulated calcein. As eluent, a NaCl solution with the same osmolarity as the calcein solution was used (250 mOsm, around 8 g of NaCl/L). Samples were kept at room temperature. For the experiments, 1 mL of the sample was divided and placed into two thin-walled glass vials. One vial was placed in a sample holder, which was connected to a water bath. The circulating water was in direct contact with the glass vial. The sample holder was placed into the bore of a superconductive magnet (Cryogenic, London, UK) with adjustable magnetic field strength of up to 5.6 T. The other vial was placed into a second water bath placed away from the magnetic field. Temperature was controlled and adjusted from two sensors inserted into the glass

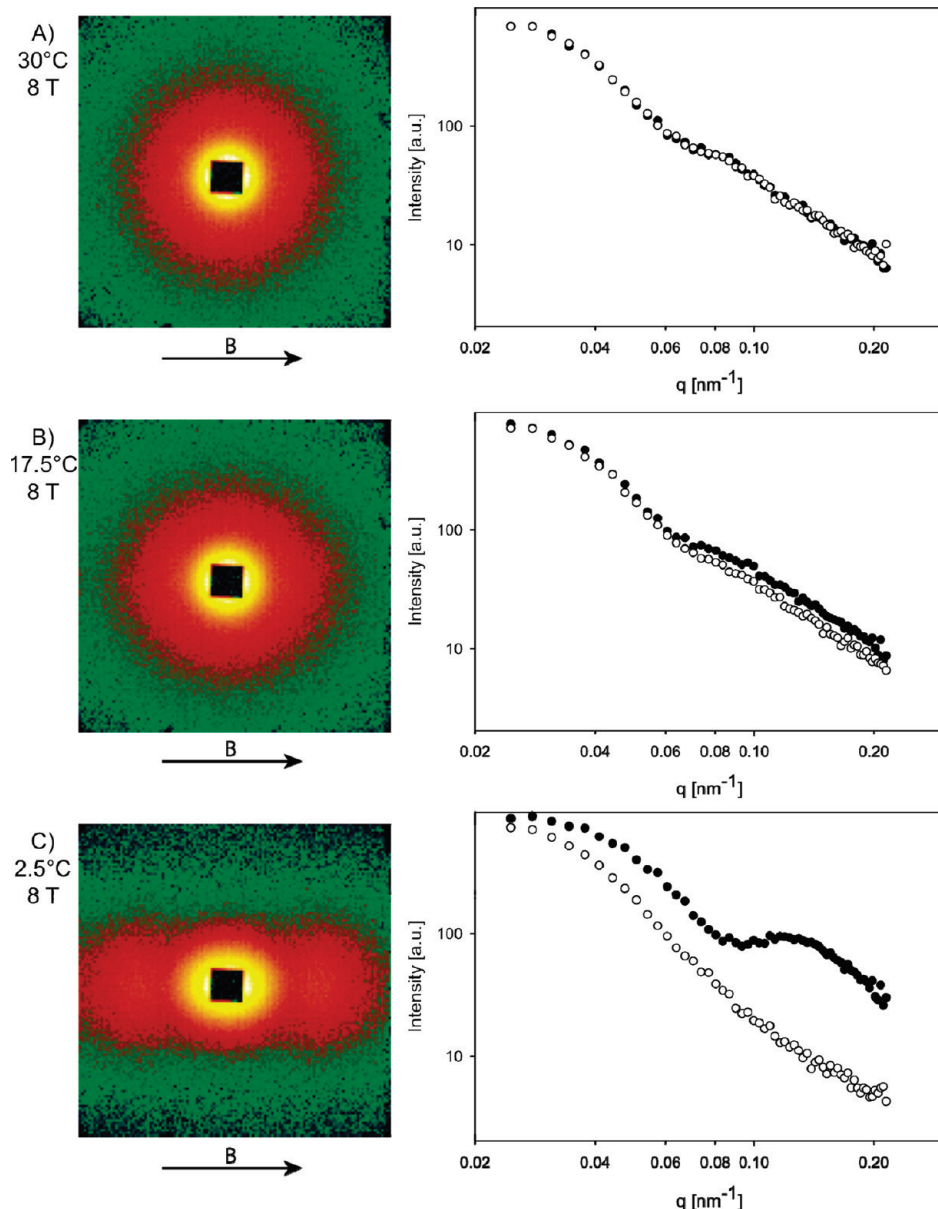


Figure 1. Effect of temperature on the 2D SANS patterns and corresponding sectoral intensity average of vesicles consisting of POPC/DMPE-DTPA·Tm in a magnetic field of 8 T. The molar ratio of POPC:DMPE-DTPA:Tm was 4:1:1, and total lipid concentration was 15 mM. Open circles: vertical 15° intensity average. Solid circles: horizontal 15° intensity average. Arrows indicate magnetic field direction.

vials. For the experiments made at 16.4 T, 1 mL of sample was divided into two NMR tubes. One was placed into the bore of the NMR magnet, the other in an external water bath.

The fluorescence of the suspension was measured with a Fluorescence Microplate Reader (Bio-Tek) at 516 nm with an excitation wavelength of 490 nm. For these measurements, 50 μ L samples were pipetted into a 96 microwell plate. Maximal fluorescence intensity I_{\max} was measured after addition of 5 μ L of Triton X-100, which initiated formation of micelles resulting in a breakdown of the vesicles. This resulted in a complete release of calcein from the vesicle interior into the bulk phase and a simultaneous increase in fluorescence.

Results

SANS Measurements. To investigate whether a magnetic field has an influence on the structure of mixed phospholipid vesicles, in which one component is doped with a strong paramagnetic agent, SANS measurements under variable mag-

netic field and temperature were carried out. Most of these measurements were performed with 100 nm vesicles composed of a mixture of POPC, DMPE-DTPA, and Tm^{3+} in a molar ratio of 4:1:1 and a total lipid concentration of 15 mM (POPC/DMPE-DTPA·Tm). Measurements were also made with 100 nm vesicles with related compositions. In POPC/highDMPE-DTPA·Tm, the amount of chelator-lipid and lanthanide was increased to a molar ratio of 3:2:2. POPE-DTPA was synthesized and used instead of DMPE-DTPA for the sample POPC/POPE-DTPA·Tm, where both lipids had the same fatty acid tails. For the POPC/DMPE-DTPA·Dy sample, Tm^{3+} was replaced by Dy^{3+} , which has an opposite sign of the magnetic anisotropy. As a comparison, POPC/DMPC, a pure phosphatidylcholine formulation, in a molar ratio of 4:1, was also investigated.

POPC/DMPE-DTPA·Tm. The effect of temperature and magnetic field strength on the scattering pattern was investigated. Figure 1 shows the 2D scattering pattern and the corresponding

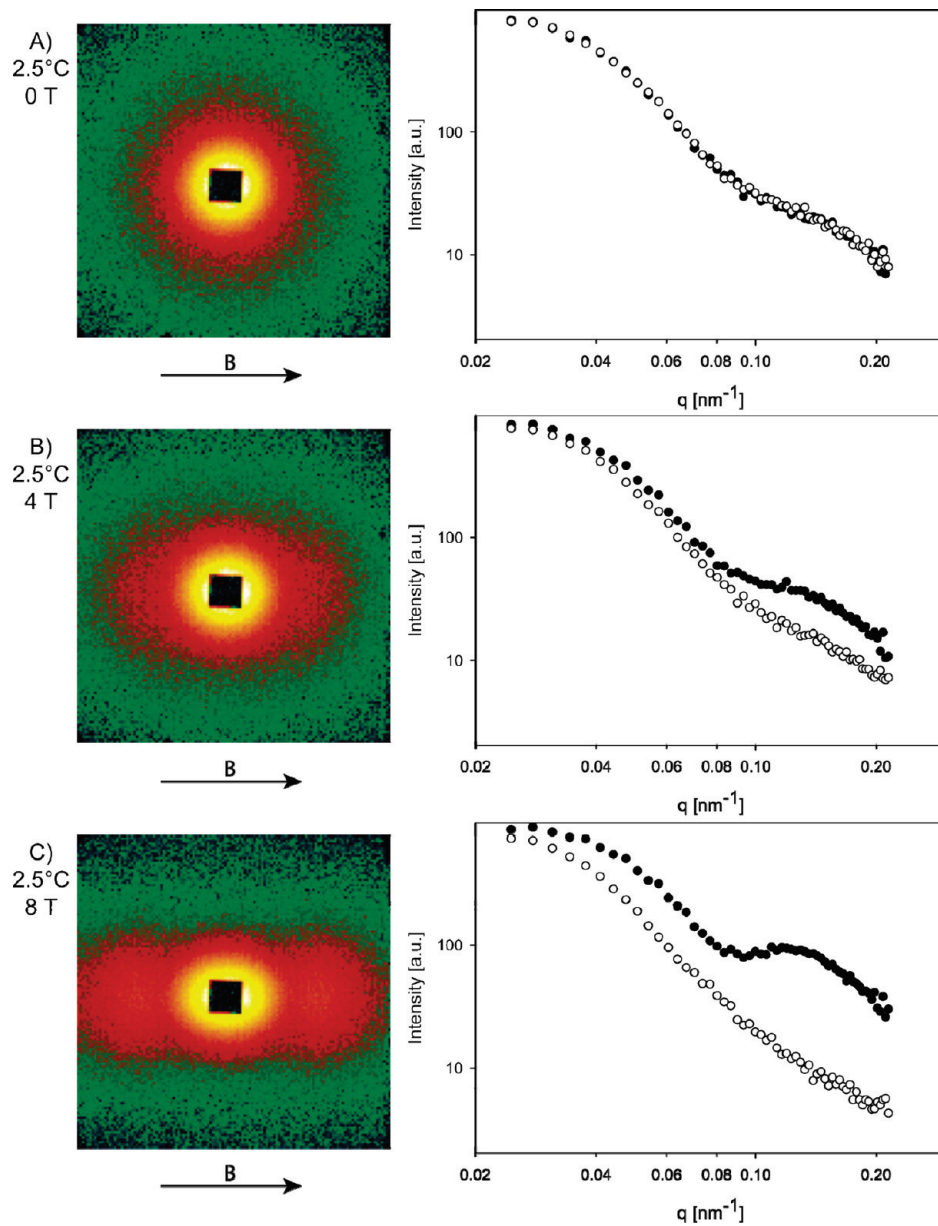


Figure 2. Effect of magnetic field strength on 2D SANS patterns and corresponding sectoral intensity average at 2.5 °C of vesicles consisting of POPC/DMPE-DTPA·Tm. The molar ratio of POPC:DMPE-DTPA:Tm was 4:1:1, and total lipid concentration was 15 mM. Open circles: vertical 15° intensity average. Solid circles: horizontal 15° intensity average. Arrows indicate magnetic field direction.

sectoral averaged curves for suspensions of POPC/DMPE-DTPA·Tm vesicles at 8 T and 2.5, 17.5, and 30 °C, all measured with a detector position at 18 m covering a q range of 0.025–0.215 nm $^{-1}$. See Supporting Information (Figure S1) for scattering pattern and sectoral averaged curves of all measured temperatures (2.5, 5, 7.5, 10, 15, 17.5, 22, and 30 °C).

The scattering pattern at 30 °C (Figure 1A) was *isotropic*, and at 17.5 °C the pattern became *anisotropic* (Figure 1B). Lowering the temperature to 2.5 °C led to an even more pronounced anisotropy in the scattering pattern (Figure 1C). This temperature-dependent increase in anisotropy was continuous (see Supporting Information for intermediate temperature steps). The scattering patterns were completely reversible in temperature without hysteresis. Additionally, cooling without the magnetic field from 30 to 2.5 °C followed by ramping of the magnet to 8 T gave the same scattering pattern as the sample which was cooled under a magnetic field (Figure 1C).

At 30 °C the SANS curves showed an inflection at 0.08 nm $^{-1}$. At lower temperatures, the inflection disappeared for the vertical

sectoral average curves (open circles) and became more distinct in the horizontal sector (closed circles). Comparison of the scattering curves furthermore indicated that a change in scattering pattern in the vertical direction was much less pronounced than in the horizontal direction.

At 2.5 °C, where the most pronounced magnetic field effect was observed, the influence of the magnetic field strength on the scattering pattern was studied. Lowering the magnetic field stepwise from 8 to 0 T led to a gradual decrease of the anisotropy in the scattering pattern ending in an isotropic pattern at 0 T. This effect was reversible in B. Figure 2 shows the scattering pattern and corresponding sectoral intensity average at a magnetic field strength of 0 T (A), 4 T (B), and 8 T (C). In addition, the SANS pattern and curves of the same sample at magnetic field strength of 2 and 6 T are shown in the Supporting Information (Figure S2).

The whole temperature range (2.5–30 °C) for vesicles consisting of POPC/DMPE-DTPA·Tm was also measured without the magnetic field. The scattering patterns were *isotropic*

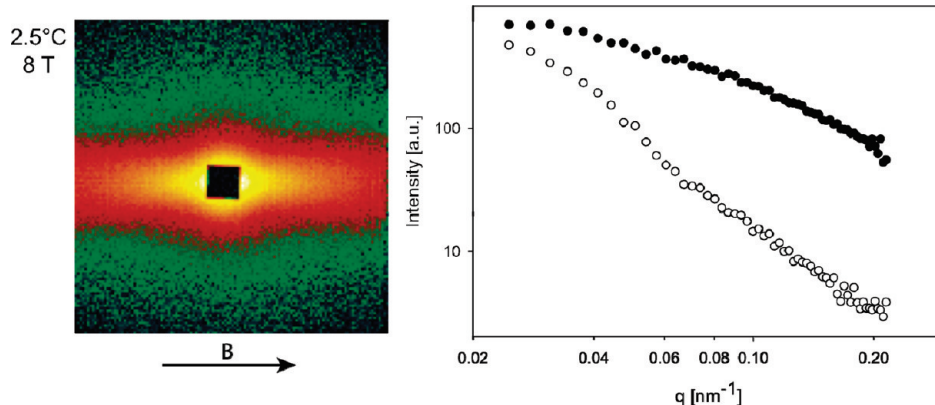


Figure 3. 2D SANS scattering pattern and corresponding sectoral intensity average at 2.5 °C and 8 T of vesicles consisting of POPC/highDMPE-DTPA complexed with Tm^{3+} . The molar ratio of POPC:DMPE-DTPA:Tm was 3:2:2, with a total lipid concentration of 15 mM. Open circles: vertical 15° intensity average. Solid circles: horizontal 15° intensity average. Arrow indicates magnetic field direction.

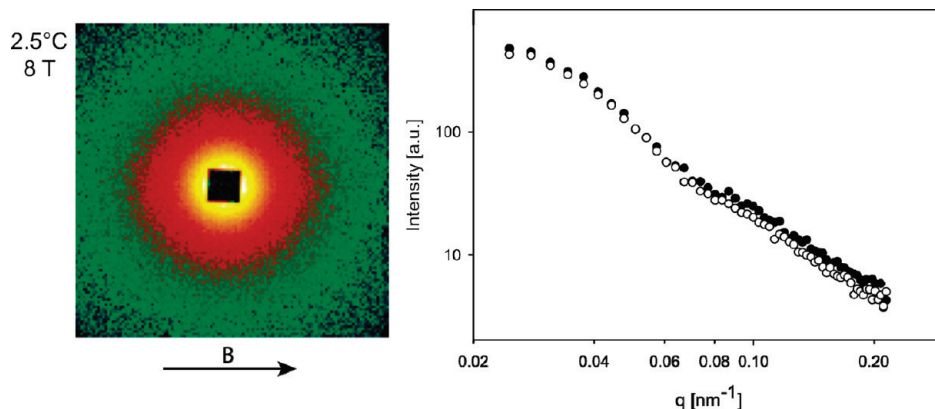


Figure 4. 2D SANS scattering pattern and corresponding sectoral intensity average at 2.5 °C and 8 T of vesicles consisting of POPC/POPE-DTPA complexed with Tm^{3+} . The molar ratio of POPC:POPE-DTPA:Tm was 4:1:1, and total lipid concentration is 15 mM. Open circles: vertical 15° intensity average. Solid circles: horizontal 15° intensity average. Arrow indicates magnetic field direction.

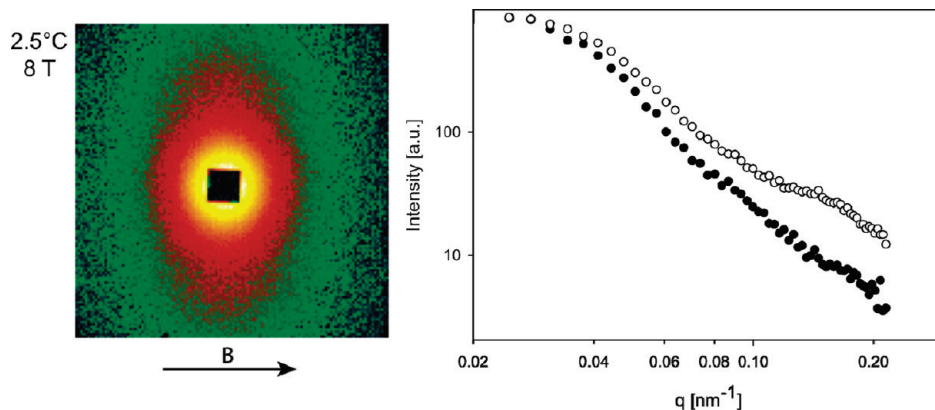


Figure 5. 2D SANS scattering patterns and corresponding sectoral intensity average at 2.5 °C and 8 T of vesicles consisting of POPC/DMPE-DTPA complexed with Dy^{3+} . The molar ratio of POPC:DMPE-DTPA:Dy was 4:1:1, and total lipid concentration is 15 mM. Open circles: vertical 15° intensity average. Solid circles: horizontal 15° intensity average. Arrow indicates magnetic field direction.

at all temperatures, which is in clear contrast to the scattering patterns observed at 8 T (see Supporting Information Figure S3 for corresponding SANS pattern and curves). All measurements indicate that the anisotropy is an effect of the magnetic field.

POPC/highDMPE-DTPA·Tm. Scattering data from vesicles with a higher molar ratio of 40% DMPE-DTPA·Tm were more anisotropic than from standard vesicles as shown in Figure 3. The measurements were carried out at 8 T and 2.5 °C, where for the standard sample the anisotropy was most pronounced.

POPC/POPE-DTPA·Tm. Replacing the chelator lipid, DMPE-DTPA, with POPE-DTPA had a strong effect on the scattering

anisotropy. The scattering pattern was only slightly anisotropic, as shown in Figure 4, measured at 8 T and 2.5 °C.

POPC/DMPE-DTPA·Dy. DMPE-DTPA·Dy has an opposite sign of the anisotropy of the paramagnetic susceptibility to DMPE-DTPA·Tm. This different magnetic property of the two lanthanides was reflected in the anisotropy of the scattering pattern of the corresponding vesicle samples. The effect of the magnetic field was investigated at 2.5 °C where the most pronounced anisotropy was observed in the scattering pattern of POPC/DMPE-DTPA·Tm (Figure 1C). SANS data collected for POPC/DMPE-DTPA·Dy under the same experimental condition showed that the anisotropy was still present but was

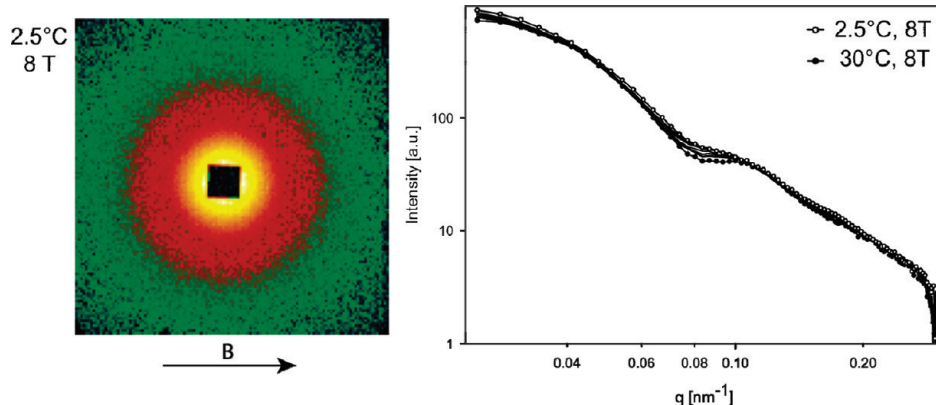


Figure 6. 2D SANS scattering pattern of vesicles consisting of POPC/DMPC at 2.5 °C (left) and radial averaged SANS curves at different temperatures (right), at 8 T. Open circles: 2.5 °C. Solid circles: 30 °C. Solid lines: temperatures in between (5, 7.5, 10, 15, 17.5, and 22 °C). Arrow indicates magnetic field direction.

now pronounced in the vertical direction (Figure 5). Again, the anisotropy of the scattering pattern increased with the magnetic field strength (see Supporting Information for SANS pattern and curves at 6 and 4 T).

POPC/DMPC. In a control measurement, mixed POPC/DMPC (molar ratio 4:1) vesicles were measured at 8 T at different temperatures between 2.5 and 30 °C. Figure 6 shows the radial averaged intensity curves of all measurements. Open circles show the data collected at 2.5 °C, and closed circles the data obtained at 30 °C. The solid lines represent the data measured in between. The scattering pattern was isotropic at all measured temperatures.

From the SANS measurements carried out, it is clear that (i) an anisotropy in the scattering pattern occurs below a critical temperature of about 22 °C only and (ii) this anisotropy can only be seen above a certain magnetic field strength of about 2 T and (iii) only if the chelator complexed with either Tm^{3+} or Dy^{3+} is present in the system.

Guinier Analysis. The SANS curves were interpreted using the Guinier analysis providing the radius of gyration, R_G . At small q values, where the overall size of the vesicle can be evaluated, R_G is equivalent to the vesicle radius and is determined using eq 1. At higher q values the Guinier analysis can be used to evaluate the membrane thickness d of the vesicle bilayer. R_G in this q -regime is determined using eq 2, with the proportionality constant c . The membrane thickness d is then $\sqrt{12}R_G$.⁴²

$$I(q) = I_0 \exp\left(-\frac{1}{3}q^2 R_G^2\right) \quad (1)$$

$$I(q) = \frac{c}{q^2} \exp(-R_G^2 q^2) \quad (2)$$

In Figure 7, diameters obtained from the Guinier analysis for different temperatures are plotted for vesicles consisting of POPC/DMPE-DTPA·Tm at 0 and 8 T and of POPC/DMPC at 8 T. For POPC/DMPE-DTPA·Tm at 0 T (Figure 7, black open circles), the diameter was around 96 nm at 30, 22, and 17.5 °C but decreased to 84.5 nm when the temperature was lowered to 2.5 °C. The same sample at 8 T (Figure 7, black closed circles) showed the same temperature dependence with a slight deviation in the measured sizes. For POPC/DMPC at 8 T (Figure 7, gray closed circles), the changes in vesicle size were less pronounced with a slight size increase at lower temperatures.

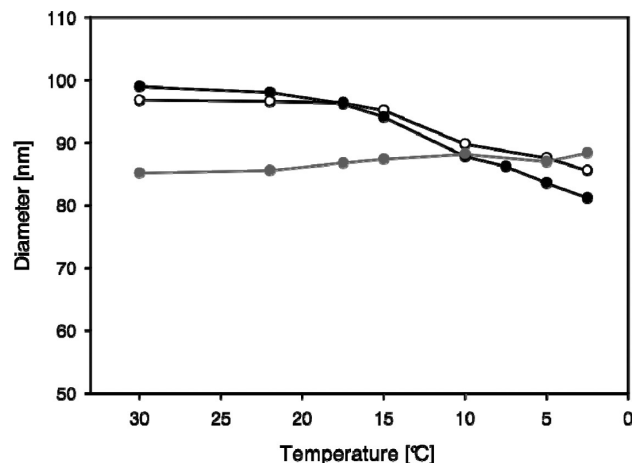


Figure 7. Vesicle diameters obtained with the Guinier analysis at different temperatures of POPC/DMPC (gray) and POPC/DMPE-DTPA·Tm (black) at 0 T (open symbols) and 8 T (closed symbols). The diameter of POPC/DMPE-DTPA·Tm decreases with decreasing temperature, while the diameter of POPC/DMPC vesicles stays more or less constant over the whole measured temperature range.

Guinier fits were also made of the sectoral averaged scattering patterns at 8 T and 2.5 °C, indicating a different vesicle diameter in magnetic field direction than perpendicular to it for POPC/DMPE-DTPA·Tm, POPC/DMPE-DTPA·Dy, and POPC/high-DMPE-DTPA·Tm (Figure 8).

In the high q range, measured at a detector distance of 2 m, the membrane thickness in direction of the magnetic field and perpendicular to the field could be determined using eq 2 for vesicles consisting of POPC/DMPE-DTPA·Tm at 2.5 °C and 8 T (Figure 9). The determined membrane thickness in field direction was 5.0 nm and perpendicular to the field was 3.6 nm.

Cryo-TEM Measurements. Cryo-TEM micrographs were taken to prove the existence of vesicles for all investigated samples, as well as to get information about the size distribution and the morphology of the vesicles. As mentioned above, for POPC/DMPE-DTPA·Tm, the neutron scattering patterns were isotropic above 17 °C and anisotropic at 17 °C and below. Cryo-TEM in the absence of a magnetic field was used to investigate whether this change in morphology can also be seen without magnetic field. We therefore froze samples held at room temperature, as well as samples held at 5 °C. Figure 10 shows the cryo-TEM micrographs of the standard sample POPC/DMPE-DTPA·Tm (A), of POPC/DMPE-DTPA·Dy (B), and of POPC/DMPC (C). In all micrographs, most of the vesicles

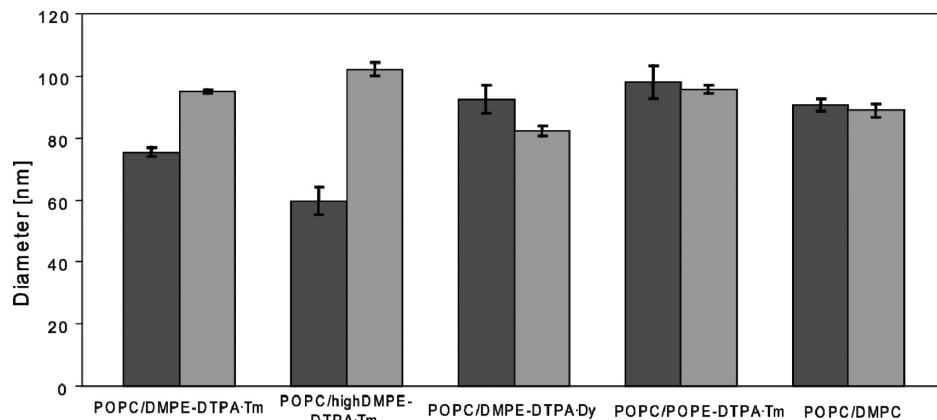


Figure 8. Vesicle diameter under a magnetic field of 8 T at 2.5 °C, derived from sectoral averaged SANS data with the Guinier analysis. Dark gray: Diameters in direction of the magnetic field. Light gray: Diameters in perpendicular direction to the magnetic field. Error bars indicate the fit uncertainty.

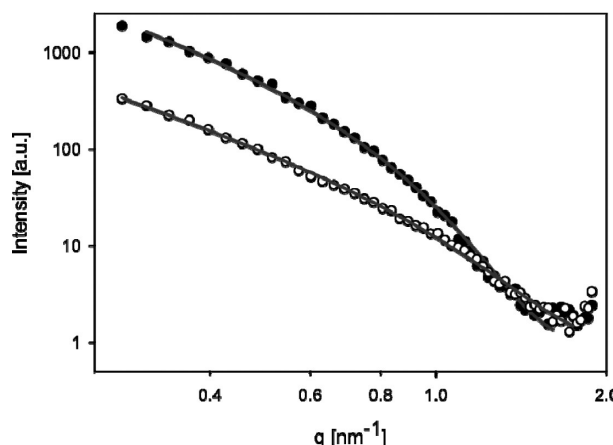


Figure 9. Sectoral averaged SANS curves at high q values of POPC/DMPE-DTPA-Tm at 8 T and 2.5 °C where the membrane thickness can be determined. Closed circles are in direction of the magnetic field; open circles are perpendicular to the field; and solid lines show corresponding Guinier fits.

were unilamellar and relatively homogeneous in size, although a few oligolamellar vesicles were found. Figure 11 shows micrographs of two other vesicle samples investigated, POPC/highDMPE-DTPA-Tm (A) and POPC/POPE-DTPA-Tm (B). Again, the vesicles were rather uniform in size and mostly unilamellar. Vesicles shown in Figure 11B were prepared with a chelator bound to a phospholipid with one unsaturated acyl chain (POPE-DTPA instead of DMPE-DTPA). Some of these vesicles had an elongated morphology.

At closer examination, the membrane of some vesicles, particularly those frozen from 5 °C, looks somewhat edged, i.e., the vesicles are not perfectly spherical, but comprises flattened membrane segments. In Figure 12, another micrograph of the standard sample (POPC/DMPE-DTPA-Tm) frozen from 5 °C as well as a zoom in of the 5 °C micrograph of Figure 10A are shown. Arrows point to the above-mentioned edged vesicles. Edged vesicles are also visible in Figures 10A–C and 11A, particularly in the 5 °C micrographs. In Figure 11B, it is difficult to find vesicles with clear edges.

^{31}P NMR. ^{31}P NMR measurements were carried out with POPC/DMPE-DTPA-La and POPC/DMPC. La^{3+} instead of Tm^{3+} or Dy^{3+} was used to prevent shifts and broadenings of the NMR line. Figure 13(A–C) shows the ^{31}P NMR spectra of POPC/DMPE-DTPA-La at 2.5, 25, and 30 °C. At low temperatures, the spectrum is a powder pattern (Figure 13C). If the temperature was raised, the isotropic peak became

increasingly pronounced (Figure 13A,B). For the pure phospholipid sample, POPC/DMPC, ^{31}P NMR spectra were taken at 2.5 and 30 °C (Figure 13, D,E). The powder pattern was again dominant at low temperatures (Figure 13E), and at 30 °C (Figure 13D), the isotropic peak was more pronounced.

Permeability Measurements. Permeability measurements were carried out with a series of vesicles containing a water-soluble fluorescence marker, calcein, which shows low fluorescence at high concentrations (fluorescence is quenched) and becomes fluorescent once it passes the membrane and gets diluted outside the vesicles. By measuring the fluorescence before and after an experiment, information was obtained about a possible leakage. The leakage of a sample exposed to a magnetic field was compared to the leakage of a sample, which experienced the same temperature profile without a magnetic field. Most permeability measurements were carried out at a magnetic field strength of 5.6 T. In addition, some samples were exposed to a magnetic field of 16.4 T. The used phospholipid formulation was POPC/DMPE-DTPA in a molar ratio of 4:1. The complexed lanthanides were either Tm^{3+} or Dy^{3+} or a mixture of the two. A variety of temperature profiles were carried out. None of the experiments showed a significant magnetic field effect on membrane permeability (data not shown). Variation in total lipid concentration or in vesicle size did not alter the results.

Discussion

The observed magnetic field dependent anisotropy of the SANS scattering pattern clearly indicates a magnetic field effect on some of the investigated vesicle formulations. We now propose an oriented domain model that considers a temperature-induced lipid demixing and domain formation, followed by magnetic field induced domain orientation. For POPC/DMPE-DTPA-Tm, a lowering of the temperature below 25 °C, which is close to the phase transition temperature T_M of DMPC (23.6 ± 1.5 °C),⁴³ leads to a demixing of the two phospholipids and the formation of DMPE-DTPA-Tm-rich domains. These domains grow as the temperature is lowered, leading to clusters of DMPE-DTPA-Tm, which have a sufficiently high magnetic susceptibility anisotropy to become oriented in a strong magnetic field. The domains align with the domain normal parallel to the magnetic field. Figure 14 depicts the oriented domain model of a basically spherical vesicle containing two flat domains. The domains are assumed to consist of a DMPE-DTPA-Tm-rich bilayer in the solid-ordered state, embedded in the POPC bilayer in the liquid-disordered state. The two domains occupy an area

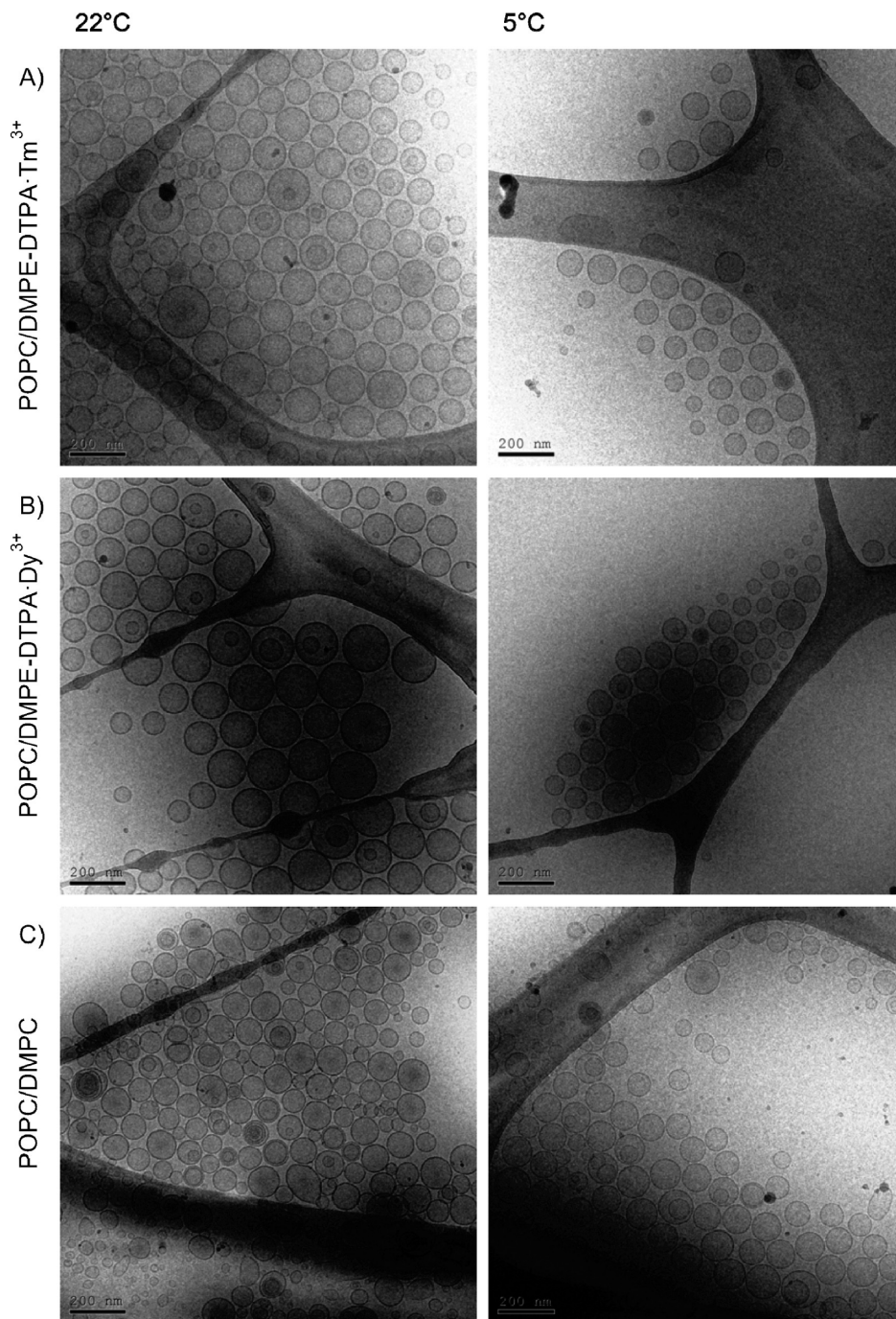


Figure 10. Cyro-TEM micrographs of vesicle suspensions taken from room temperature (left column) and from 5 °C (right column). Vesicles consisting of (A) POPC:DMPE-DTPA:Tm³⁺ (4:1:1 molar ratio), (B) POPC:DMPE-DTPA:Dy³⁺ (4:1:1 molar ratio), and (C) POPC:DMPC (4:1 molar ratio) are shown. The total lipid concentration was 15 mM in all samples. Scale bar = 200 nm.

of 20% of the total vesicle surface, in approximation of the 4:1:1 molar ratio of POPC:DMPE-DTPA:Tm used. Tm³⁺, which confers a large magnetic moment to the membrane, is concentrated in the domain, making orientation with the domain normal perpendicularly to the magnetic field possible.

The fact that an identical scattering pattern of the vesicles at 8 T and 2.5 °C (Figure 1C) is obtained, regardless of whether the magnetic field is turned on before or after cooling the sample, indicates that the *temperature decrease* is responsible for the structural anisotropy, which can then be oriented by magnetic fields. We propose that this structural anisotropy is caused by lateral segregation of the two lipids in the system, providing a temperature-dependent miscibility of DMPE-DTPA in POPC. Temperature-induced lateral segregation or demixing of multicomponent phos-

pholipid membranes is well documented. Most literature describes ternary mixtures of two phospholipids with different phase transition temperatures and cholesterol.^{24,26,28,29,31,33,35,36,44} Three distinct phase morphologies for giant unilamellar vesicles have been detected by fluorescence microscopy.³⁵ Below a certain miscibility temperature, a phase separation of the two phospholipids occurs. If cholesterol is present, two coexisting liquid phases are formed. Without cholesterol, the higher melting lipid forms a solid domain in a liquid phase. Such solid domains assume the form of flat plates.³⁰ Lipid domains have also been found on small unilamellar vesicles by SANS using a contrast matching technique with chain-deuterated phospholipids.^{24,28,31,33,44} Hartmann et al.²⁷ have reported direct visualization of lipid domains on giant vesicles by freeze-etch electron microscopy.

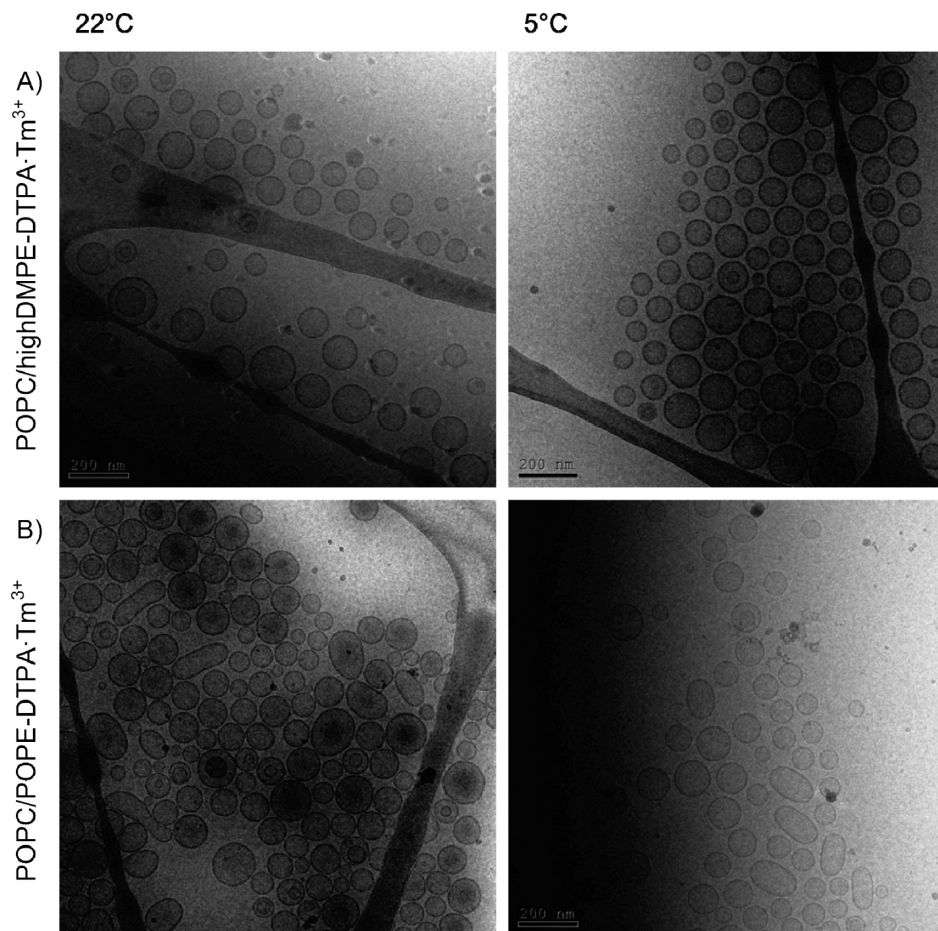


Figure 11. Cryo-TEM micrographs of vesicle suspensions taken from room temperature (left column) and from 5 °C samples (right column). Vesicles consisting of (A) POPC:DMPE-DTPA:Tm³⁺ (3:2:2 molar ratio) and (B) POPC:POPE-DTPA:Tm³⁺ (4:1:1 molar ratio) are shown. The total lipid concentration was 15 mM in all samples. Scale bar = 200 nm.

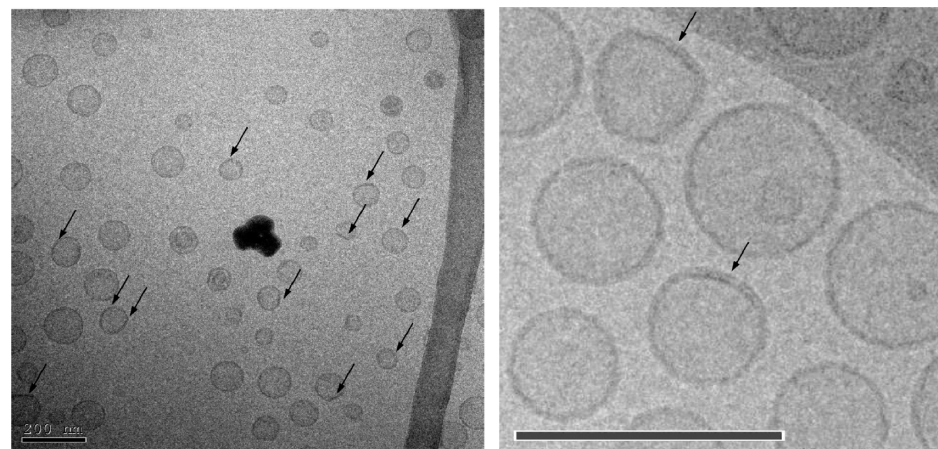


Figure 12. Cryo-TEM micrographs of vesicles consisting of POPC/DMPE-DTPA-Tm in a molar ratio of 4:1:1 taken from samples frozen from 5 °C. Arrows point to edges in the membrane of the vesicles. Right: Zoom of 5 °C micrograph in Figure 10A. Scale bar = 200 nm.

Close observation of our cryo-TEM micrographs made evident that the vesicles were not perfectly spherical but often show edges in the membrane, which we attribute to solid domains of the higher-melting lipid (Figure 12). In comparison, these edges seem to appear more frequently in samples frozen from 5 °C than in samples frozen from 22 °C (Figures 10 and 11). The only exception was POPC/POPE-DTPA-Tm, where no clear edges could be identified (Figure 11B). This is reasonable since the unsaturated chain in POPE-DTPA is expected to lower the chain melting temperature.

A strong indicator for lateral segregation is the difference in membrane thickness horizontal and perpendicular to the magnetic field direction at 8 T and 2.5 °C, as found by the Guinier analysis of the SANS data of the POPC/DMPE-DTPA-Tm sample (Figure 9). The membrane thickness parallel to the magnetic field was 3.5 nm and perpendicular to the field was 5.0 nm. Previously, the bilayer thickness of POPC was determined by Kucerka et al.,⁴⁵ and a value of 3.82 nm was obtained. This is similar to the thickness we measured parallel to the magnetic field (3.5 nm). The bilayer thickness of DMPC

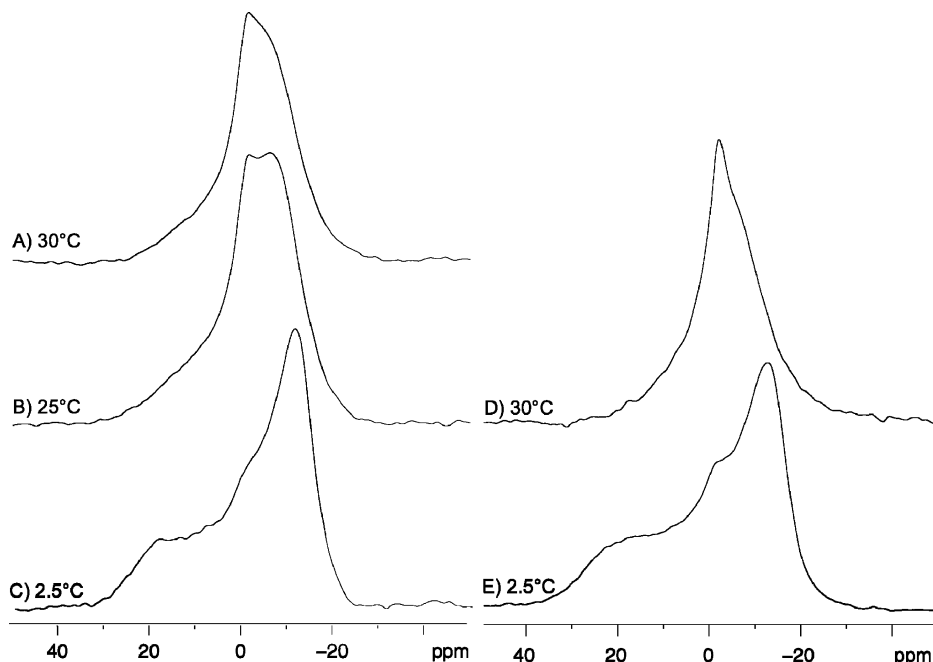


Figure 13. Left: ^{31}P NMR spectra of POPC:DMPE-DTPA·La recorded at 30 °C (A), 25 °C (B), and 2.5 °C (C). Right: ^{31}P NMR spectra of POPC/DMPC recorded at 30 °C (D) and 2.5 °C (E). The powder pattern dominates the spectrum at low temperature, whereas at higher temperatures the isotropic peak is more pronounced.

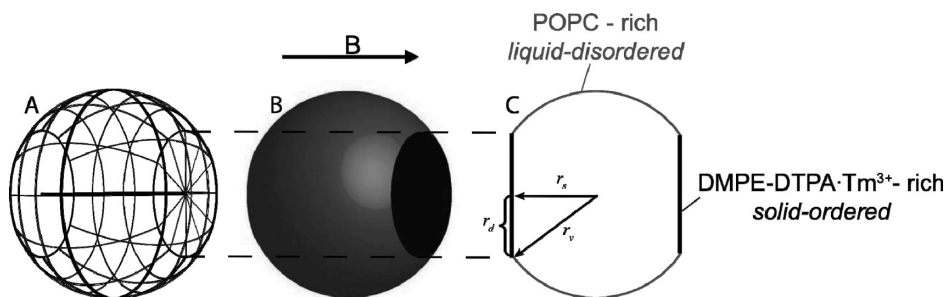


Figure 14. Sketch illustrating the magnetic field alignable domain model. A, B, and C show three drawings of a vesicle with two flat domains. DMPE-DTPA·Tm is assumed to form solid domains (black in B and C) in a solid-ordered state, surrounded by POPC (gray in B and C) in the liquid-disordered state. r_v is the vesicle radius; r_d is the domain radius; and r_s is the vesicle short radius in direction of the domain.

at 10 °C was found by Pencer et al.⁴⁶ to be 4.43 nm, and the radius of DTPA complexed with the lanthanide gadolinium is 2.95 Å.⁴⁷ It is therefore expected that the thickness of a DMPE-DTPA·Tm bilayer at 2.5 °C is more than 4.5 nm, corresponding to the value which we observed for the bilayer thickness perpendicular to the magnetic field (5.0 nm). In any case, without knowing the precise configuration of the DMPE-DTPA·Tm headgroup, it can still be expected that DMPE-DTPA in the solid-ordered state forms a significantly thicker bilayer than POPC in the liquid-disordered state, corresponding with the determined thickness differences parallel and perpendicular to the magnetic field.

According to our model, the anisotropy of the SANS pattern has two origins. First, the scattering length density of DMPE-DTPA·Tm is different from the one of POPC. We estimated the scattering length density of DMPE-DTPA·Tm in the solid-ordered state to be $1.10 \times 10^{10} \text{ cm}^{-2}$ (refs 47–50) and of POPC in the liquid-disordered state to be $2.51 \times 10^9 \text{ cm}^{-2}$ (refs 32 and 51). Therefore, demixing of the lipids yields anisotropic scattering. Second, the average vesicle size seen by SANS in the horizontal direction is smaller than in the vertical direction, due to the flattened curvature of the domains, increasing the anisotropy of the neutron scattering. Figure 7 shows that the Guinier size of the vesicles follows the same temperature

dependence with and without magnetic field, with a maximal difference of 5% at 2.5 °C. Guinier fits of sectoral averaged SANS curves of samples with an anisotropic scattering pattern clearly show a different radius in the direction of the magnetic field compared to the radius perpendicular to the magnetic field (Figure 8). This is a clear indication that the samples were not perfectly spherical at low temperatures.

Some considerations can be made to compare vesicle diameter obtained by Guinier analysis perpendicular and parallel to the magnetic field with the expected diameter reduction due to rigid domains, which represent flat membrane segments. For the vesicles consisting of POPC/DMPE-DTPA·Tm and POPC/DMPE-DTPA·Dy, we assumed that the area of the domain, A_{Domain} , accounts for 20% of the total vesicle surface, A_{Vesicle} , and for 40% for POPC/highDMPE-DTPA·Tm, according to the amount of chelator-lipid (DMPE-DTPA) in the samples. Using eqs 3, 4, and 5 and assuming a vesicle radius r_v of 50 nm, the short vesicle radius in the direction of the domain r_s can be calculated.

$$A_{\text{Vesicle}} = 4\pi r_v^2 \quad (3)$$

$$A_{\text{Domain}} = \pi r_{\text{d}}^2 \quad (4)$$

$$r_{\text{v}}^2 = r_{\text{d}}^2 + r_{\text{s}}^2 \quad (5)$$

According to the magnetic field alignable domain model (Figure 14), the domains doped with Tm³⁺ orient with their normal parallel to the magnetic field, resulting in a reduced diameter in this direction ($d_{\parallel} = r_{\text{s}} + r_{\text{v}}$ assuming one domain, $d_{\parallel} = 2r_{\text{s}}$ assuming two domains). In contrast, for domains doped with Dy³⁺, the short diameter would be perpendicular to the magnetic field as shown in Table 1.

For vesicles consisting of POPC/DMPE-DTPA·Tm, the theoretically assumed reduction of the diameter parallel to the magnetic field is in good agreement with the diameter obtained by the Guinier analysis. For POPC/highDMPE-DTPA·Tm, the theoretical short vesicle radius assuming two flat domains (44.8 nm) is smaller compared with the diameter obtained by the Guinier analysis (59.6 nm). This could indicate that more than two domains are formed with increasing amounts of DMPE-DTPA·Tm.

For POPC/DMPE-DTPA·Dy, the diameters obtained by the Guinier analysis were 92.4 and 82.2 nm, and in this case the smaller diameter was measured perpendicular to the magnetic field. Comparison of Figure 5 with Figure 1A shows that the scattering pattern of DMPE-DTPA·Dy is not identical to the scattering pattern of DMPE-DTPA·Tm rotated by 90°, as the anisotropy is less pronounced. According to our model, the POPC/DMPE-DTPA·Dy sample undergoes the same temperature-driven domain formation, with the domain normal oriented perpendicular to the magnetic field. This explains the 90° shift in the anisotropy of the scattering pattern. Domains oriented perpendicular to the magnetic field have an additional degree of freedom, as they can rotate around an axis parallel to the magnetic field. This explains the less pronounced scattering anisotropy of POPC/DMPE-DTPA·Dy compared to POPC/DMPE-DTPA·Tm, as well as the underestimation of the vesicle radius perpendicular to the magnetic field in the calculation.

The POPC/highDMPE-DTPA·Tm sample shows a much more pronounced anisotropy than POPC/DMPE-DTPA·Tm, indicating larger and more pronounced domain formation (Figure 3). Domain formation may also occur for POPC/DMPC as edges in the cryo-TEM micrographs indicate (Figure 10C), but they cannot be oriented without lanthanides (see isotropic scattering pattern for POPC/DMPC in Figure 6). In POPC/POPE-DTPA·Tm, no evidence of domain formation was found (SANS, Figure 4; cryo-TEM, Figure 11B). This could be due to the fact that the temperatures investigated were above the phase transition temperatures of both lipids, which are below 0 °C.³⁸ A sample consisting of DMPC/DMPE-DTPA·Tm,

where the phase transition temperature of both lipids is around room temperature, was shown to form flat disks—and not vesicles—as discussed elsewhere.⁴⁰

We used ³¹P NMR to confirm that the sample morphology was purely vesicular at the temperatures where anisotropic SANS patterns were obtained and that no structures were formed which had evaded the cryo-TEM analysis. ³¹P NMR spectra of POPC/DMPE-DTPA·Tm and POPC/DMPE-DTPA·Dy were difficult to interpret because of line shift and line broadening (data not shown). Instead, we show spectra recorded of POPC/DMPE-DTPA·La, where the diamagnetic La³⁺ was complexed to the chelator instead of Tm³⁺ or Dy³⁺. This sample lost its magnetic orientability and gave spectra similar to those of POPC/DMPC. ³¹P NMR measurements of POPC/DMPE-DTPA·La were made at 2.5, 25, and 30 °C and of POPC/DMPC at 2.5 and 30 °C (Figure 13). For both samples, a powder pattern with very small isotropic contribution at 0 ppm was obtained at 2.5 °C, which is in agreement with the purely vesicular structure found with cryo-TEM. At 25 and 30 °C, the isotropic peak became more dominant, representing faster lipid motion. For POPC/DMPE-DTPA·La, NMR spectra were recorded in the following order: 25 °C, 2.5 °C, 25 °C, 30 °C, and 25 °C. The three spectra at 25 °C were identical, indicating that no irreversible structure changes happened during heating or cooling of the sample, confirming the reversibility of the SANS measurements.

With respect to our considerations before starting the measurement (see Introduction), it is worth noting that the following potential magnetic field effects were not observed: vesicle aggregation/fusion, vesicle budding/fission, and alteration of bilayer permeability. Fusion, fission, or aggregation would lead to a change in size distribution. We have monitored the size distribution with DLS, SANS, and cryo-TEM. SANS and cryo-TEM results indicated a slight decrease in vesicle size when the temperature was lowered (SANS, Figure 7; cryo-TEM, see Supporting Information, Figure S5) contradicting fusion and aggregation. Significant aggregation, fusion, or fission of vesicles would have led to a more drastic size change and were not observed in the cryo-TEM micrographs. DLS measurements carried out before and after the SANS measurements showed that no irreversible change in size distribution had occurred (data not shown). It appears improbable that fusion, fission, or aggregation would be totally reversible. Furthermore, fusion and fission could not explain the structural anisotropy required for magnetic orientation.

Budding vesicles would also represent an anisotropic structure. Even though no proof against magnetic field induced budding for our samples can be given, we found no result supporting it. While temperature-induced²⁶ or photo-induced⁵² budding was observed for giant vesicles, budding is not likely to happen for energetical reasons in the case of

TABLE 1: Comparison of Guinier Vesicle Diameters Perpendicular d_{\perp} and Parallel d_{\parallel} to the Magnetic Field with Expected Diameters Assuming One or Two Flat Domains, Which Are Oriented in the Magnetic Field

	POPC/DMPE-DTPA·Tm		POPC/highDMPE-DTPA·Tm		POPC/DMPE-DTPA·Dy	
	vesicle diameter [nm]		vesicle diameter [nm]		vesicle diameter [nm]	
	d_{\perp}	d_{\parallel}	d_{\perp}	d_{\parallel}	d_{\perp}	d_{\parallel}
assuming one domain	100	72.4	—	—	72.4	100
assuming two domains	100	77.4	100	44.8	77.4	100
Guinier diameter	95.1	75.3	102.1	59.6	82.2	92.4

For POPC/highDMPE-DTPA·Tm, the assumption of one flat domain leads to a domain radius r_{d} of 63.2 nm, which is larger than the vesicle radius, making this assumption less probable. Guinier diameters were obtained from fitting sectoral averaged SANS data at 2.5 °C and 8 T perpendicular and parallel to the magnetic field.

small unilamellar vesicles with their highly curved membranes.³⁰ Additionally, no hint for budding of vesicles without magnetic field could be found in cryo-TEM micrographs (Figures 10 and 11).

The anisotropy required for magnetic orientation could have been explained by vesicle aggregates with a nonspherical overall shape but has not been observed, as mentioned above. Another possible explanation for the anisotropy could have been the deformation of vesicles from spherical to ellipsoidal shape. Comparison of cryo-TEM micrographs obtained from samples frozen from 5 °C and from room temperature showed no temperature-induced ellipsoidal deformation of any sample investigated, contradicting a possible magnetic field orientation after ellipsoidal deformation caused by low temperatures (Figures 10 and 11). Some ellipsoidal vesicles consisting of POPC/POPE-DTPA·Tm were found at both temperatures (Figure 11B). However, no significant anisotropy in scattering pattern was found for this sample (Figure 4). Fitting of SANS data with an ellipsoidal shell form factor could not satisfactorily describe the SANS curves.

Leakage measurements of calcein through the vesicle membrane showed no effect of the magnetic field on membrane permeability. Lowering the temperature below room temperature increased the permeability of all the samples tested. Leakage occurs preferentially at packing defects in the bilayer structure.⁵³ Such defects are found at the edges of domains. The fact that the magnetic field has no influence on the permeability of the vesicles is a further indication that the domain formation itself is not influenced by the magnetic field but by temperature. The domains could then reposition themselves in the POPC membrane to achieve a lowest-energy state, with an orientation depending on the lanthanide used.

Conclusion

We have shown that vesicles consisting of mixtures of POPC and DMPE-DTPA complexed with paramagnetic lanthanides (Tm^{3+} , Dy^{3+}) react to magnetic fields at low temperatures (below 17 °C). This reactivity originates from a demixing of the two lipids at a temperature below 17 °C, leading to solid-ordered domains rich in DMPE-DTPA·lanthanide surrounded by POPC in the fluid-disordered state. This demixing is independent of whether a magnetic field is applied or not. The domains formed have the shape of flat disks and assemble the large magnetic moments conferred by the lanthanides. The whole domain thus becomes orientable in the magnetic field. The direction of alignment can be selected with the type of paramagnetic lanthanide ion used. The domains orient with their normal perpendicular to the field with Dy^{3+} and parallel to the field with Tm^{3+} .

Acknowledgment. The authors acknowledge EMEZ for technical support.

Supporting Information Available: Additional SANS data, including scattering pattern and sectoral averaged curves of all measured temperatures and magnetic field strength of POPC/DMPE-DTPA·Tm and POPC/DMPE-DTPA·Dy. Dynamic light scattering (DLS) measurements in comparison with size analysis obtained from cryo-TEM. This material is available free of charge via the Internet at <http://pubs.acs.org>.

References and Notes

- (1) Qiu, X. X.; Mirau, P. A.; Pidgeon, C. *Biochim. Biophys. Acta* **1993**, *1147*, 59–72.
- (2) Speyer, J. B.; Sripada, P. K.; Dasgupta, S. K.; Shipley, G. G.; Griffin, R. G. *Biophys. J.* **1987**, *51*, 687–691.
- (3) De Angelis, A. A.; Opella, S. J. *Nat. Protocols* **2007**, *2*, 2332–2338.
- (4) Katsaras, J.; Harroun, T. A.; Pencer, J.; Nieh, M. P. *Naturwissenschaften* **2005**, *92*, 355–366.
- (5) Triba, M. N.; Warschawski, D. E.; Devaux, P. F. *Biophys. J.* **2005**, *88*, 1887–1901.
- (6) van Dam, L.; Karlsson, G.; Edwards, K. *Biochim. Biophys. Acta* **2004**, *1664*, 241–256.
- (7) Katsaras, J.; Donaberger, R. L.; Swainson, I. P.; Tennant, D. C.; Tun, Z.; Vold, R. R.; Prosser, R. S. *Phys. Rev. Lett.* **1997**, *78*, 899.
- (8) Prosser, R. S.; Hunt, S. A.; DiNatale, J. A.; Vold, R. R. *J. Am. Chem. Soc.* **1996**, *118*, 269–270.
- (9) Binnemans, K.; Gorller-Walrand, C. *Chem. Rev.* **2002**, *102*, 2303–2345.
- (10) Prosser, R. S.; Volkov, V. B.; Shiyanovskaya, I. V. *Biochem. Cell Biol.* **1998**, *76*, 443–451.
- (11) Prosser, R. S.; Volkov, V. B.; Shiyanovskaya, I. V. *Biophys. J.* **1998**, *75*, 2163–2169.
- (12) Rodriguez-Castañeda, F.; Haberz, P.; Leonov, A.; Griesinger, C. *Magn. Reson. Chem.* **2006**, *44*, S10–S16.
- (13) Tolman, J. R.; Flanagan, J. M.; Kennedy, M. A.; Prestegard, J. H. *Proc. Natl. Acad. Sci. U.S.A.* **1995**, *92*, 9279–9283.
- (14) Zhuang, T. D.; Lee, H. S.; Imperiali, B.; Prestegard, J. H. *Protein Sci.* **2008**, *17*, 1220–1231.
- (15) Grant, C. W. M.; Karlik, S.; Florio, E. *Magn. Reson. Med.* **1989**, *11*, 236–243.
- (16) Brumm, T.; Mops, A.; Dolinsky, C.; Bruckner, S.; Bayerl, T. M. *Biophys. J.* **1992**, *61*, 1018–1024.
- (17) Helfrich, W. *Phys. Lett. A* **1973**, *A 43*, 409–410.
- (18) Kiselev, M. A.; Gutberlet, T.; Hoell, A.; Aksenov, V. L.; Lombardo, D. *Chem. Phys.* **2008**, *345*, 181–184.
- (19) Kiselev, M. A.; Zemlyanaya, E. V.; Aswal, V. K.; Neubert, R. H. H. *Eur. Biophys. J.* **2006**, *35*, 477–493.
- (20) Reinh, H.; Brumm, T.; Bayerl, T. M. *Biophys. J.* **1992**, *61*, 1025–1035.
- (21) Liburdy, R. P.; Tenforde, T. S.; Magin, R. L. *Radiat. Res.* **1986**, *108*, 102–111.
- (22) Tenforde, T. S.; Liburdy, R. P. *J. Theor. Biol.* **1988**, *133*, 385–396.
- (23) Kurashima, H.; Abe, H.; Ozeki, S. *Mol. Phys.* **2002**, *100*, 1445–1450.
- (24) Anghel, V. N. P.; Kucerka, N.; Pencer, J.; Katsaras, J. *J. Appl. Crystallogr.* **2007**, *40*, 513–525.
- (25) Bacia, K.; Schwille, P.; Kurzchalia, T. *Proc. Natl. Acad. Sci. U.S.A.* **2005**, *102*, 3272–3277.
- (26) Baumgart, T.; Hess, S. T.; Webb, W. W. *Nature* **2003**, *425*, 821–824.
- (27) Hartmann, W.; Galla, H. J.; Sackmann, E. *FEBS Lett.* **1977**, *78*, 169–172.
- (28) Imai, M.; Masui, T.; Yanagisawa, M. *Reports of the Institute of Fluid Science*; Tohoku University, 2007, 1–5.
- (29) Korlach, J.; Schwille, P.; Webb, W. W.; Feigenson, G. W. *Proc. Natl. Acad. Sci. U.S.A.* **1999**, *96*, 8461–8466.
- (30) Lipowsky, R.; Dimova, R. *J. Phys.: Condens. Matter* **2003**, *15*, S31–S45.
- (31) Masui, T.; Imai, M.; Urakami, N. *Physica B* **2006**, *385*, 821–823.
- (32) Pencer, J.; Jackson, A.; Kucerka, N.; Nieh, M. P.; Katsaras, J. *Eur. Biophys. J. Biophys. Lett.* **2008**, *37*, 665–671.
- (33) Pencer, J.; Mills, T.; Anghel, V.; Krueger, S.; Epand, R. M.; Katsaras, J. *Eur. Biophys. J. E* **2005**, *18*, 447–458.
- (34) Seifert, U. *Phys. Rev. Lett.* **1993**, *70*, 1335–1338.
- (35) Veatch, S. L.; Keller, S. L. *Phys. Rev. Lett.* **2002**, *89*.
- (36) Yanagisawa, M.; Imai, M.; Masui, T.; Komura, S.; Ohta, T. *Biophys. J.* **2007**, *92*, 115–125.
- (37) Torchilin, V. P.; Weissig, V.; Martin, F. J.; Heath, T. D.; New, R. R. C., *Liposomes: A Practical Approach*, 2nd ed.; Torchilin, V. P., Weissig, V., Eds.; 2003.
- (38) Walde, P.; Ichikawa, S. *Biomol. Eng.* **2001**, *18*, 143–177.
- (39) Mui, B.; Chow, L.; Hope, M. J. *Methods Enzymol.* **2003**, *367*, 3–14.
- (40) Beck, P.; Liebi, M.; Kohlbrecher, J.; Ishikawa, T.; Rüegger, H.; Fischer, P.; Walde, P.; Windhab, E. *Langmuir* **2010**; DOI: 10.1021/la903806a.
- (41) Allen, T. M. Calcein as a tool in liposome methodology. In *Liposome Technology*; Gregoriadis, G., Ed.; CRC Press: Boca Raton, 1984; Vol. 3, pp 177–182.
- (42) Hjelm, R. P.; Schteingart, C. D.; Hofmann, A. F.; Thiagarajan, P. *J. Phys. Chem. B* **2000**, *104*, 197–211.

- (43) Koynova, R.; Caffrey, M. *Biochim. Biophys. Acta* **1998**, *1376*, 91–145.
- (44) Pencer, J.; Anghel, V. N. P.; Kucerka, N.; Katsaras, J. *J. Appl. Crystallogr.* **2007**, *40*, 771–772.
- (45) Kucerka, N.; Tristram-Nagle, S.; Nagle, J. F. *J. Membr. Biol.* **2006**, *208*, 193–202.
- (46) Pencer, J.; Nieh, M. P.; Harroun, T. A.; Krueger, S.; Adams, C.; Katsaras, J. *Biochim. Biophys. Acta* **2005**, *1720*, 84–91.
- (47) Bammer, R.; de Crespigny, A. J.; Howard, D.; Seri, S.; Hashiguchi, Y.; Nakatani, A.; Moseley, M. E. *Magn. Reson. Imaging* **2004**, *22*, 619–624.
- (48) Knoll, W.; Haas, J.; Stuhrmann, H. B.; Fulldner, H. H.; Vogel, H.; Sackmann, E. *J. Appl. Crystallogr.* **1981**, *14*, 191–202.
- (49) Nagle, J. F.; Tristram-Nagle, S. *Biochim. Biophys. Acta* **2000**, *1469*, 159–195.
- (50) Tristram-Nagle, S.; Liu, Y. F.; Legleiter, J.; Nagle, J. F. *Biophys. J.* **2002**, *83*, 3324–3335.
- (51) Vacklin, H. P.; Tiberg, F.; Thomas, R. K. *Biochim. Biophys. Acta* **2005**, *1668*, 17–24.
- (52) Ishii, K.-i.; Hamada, T.; Hatakeyama, M.; Sugimoto, R.; Nagasaki, T.; Takagi, M. *ChemBioChem* **2009**, *10*, 251–256.
- (53) Ono, A.; Takeuchi, K.; Sukenari, A.; Suzuki, T.; Adachi, I.; Ueno, M. *Biol. Pharm. Bull.* **2002**, *25*, 97–101.

JP907442E